Mathematics

AIMS Mathematics, 9(7): 17932–17954.
DOI: 10.3934/math.2024873
Received: 16 March 2024
Revised: 26 April 2024
Accepted: 29 April 2024
Published: 27 May 2024

https://www.aimspress.com/journal/Math

Research article

Impact of the climate variations in nonlinear topographies on some vast oceans

Mustafah Abou-Dina[1] and Amel Alaidrous[2,*]

[1] Department of Mathematics, Faculty of Science, Cairo University, Giza 12631, Egypt
[2] Department of Mathematics, Faculty of Sciences, Umm Al-Qura University, P.O. Box 4454, Makkah21955, Saudi Arabia

* **Correspondence:** Email: aaaidrous@uqu.edu.sa.

Abstract: We study the non-linear transient gravity waves inside vast oceans with general topographies. These waves are generated following climate variations simulated by an external pressure acting on the ocean's surface. We use a perturbation method for the study. The present approach necessitates a mild slope of the topography. Quadratic solutions are obtained from nonlinear theory technique and illustrated. The reliability of the nonlinear (quadratic) solution is examined by a comparison between the trace of the bottom and the lowest streamline. The proposed model is shown to be strongly efficient in simulating the considered phenomenon, especially if the slope of the topography is not sharp. The features of the phenomenon under consideration are revealed and discussed mathematically and physically according to the nonlinear theory technique.

Keywords: climate variations; potential flow; nonlinear gravity waves; linear theory; nonlinear theory; irregular topography; integral transform
Mathematics Subject Classification: 31B10, 34G20, 37N10, 37N30

1. Introduction

Phenomena occurring in oceans are closely related to certain geological aspects as well as to meteorology and climate conditions (pressure, winds, temperature, storms, ...). Volcanic eruptions, underwater explosions and earthquakes, and testing with nuclear weapons at sea are some of the reasons for the generation of tsunamis in large oceans (see for example LeMéhauté & Wang [1] and

Abou-Dina & Hassan [2] and references included therein). On the other hand, winds, atmospheric pressure, and temperature variations, and strong storms have the potential to generate surface waves in oceans (Young [3], Holthuijsen [4]).

After their generation by the wind, ocean surface waves can travel over long distances. The propagation of such waves depends not only on the generation conditions but also on the nature of the topography of the ocean's bottom. These waves have a large impact on offshore structures, ships, coastal erosion, and sedimentation, as well as harbors. Bottom friction's effect on offshore propagating geostrophic alongshore flow explains the coastal poleward alongshore flow, highlighting the connection between ocean bottom topography and Earth's climate are discussed by Jayne et al. [5]. Seasonal variability in ocean bottom topography affects regions like subpolar and subtropical basins, leading to alternations of low and high anomalies are studied by Chen et al. [6]. Qin et al. [7] has discussed the impact of climate dynamics into the interannual variability of ocean bottom pressure in the South Pacific region. The study uses observations and models to explore the causes of observed sea level variability in the midlatitude South Pacific on interannual time scales, emphasizing the role of topography in shaping seasonal ocean bottom pressure variability. Yang and Chen [8] have discussed the significance of wind stress as a key driver of the primary along-shelf flows in the Northwest Atlantic. Du et al. [9] have focused on the simultaneous measurement of ocean surface current, vector wind, and temperature which advancing our knowledge of ocean processes and their role in shaping global climate patterns. Alaidrous [10] has discussed the impact of a floating ship in the reflection and transmission of water waves in some vast oceans and proposed a model of the water wave flow under a floating body of an incident wave in a liquid.

Several models have been elaborated to simulate the phenomenon of gravity wave propagation over a flat bottom (see for example the experimental work of, Shi et al. [11], Wang et al. [12], Bazilevskii et al. [13], De Serioa & Mossa [14] and the theoretical work of Abou-Dina [15], Abou-Dina and Helal [16, 17], Hassan [18] and references included in these publications). Lamb [19], Abou-Dina & Hassan [20], Abou-Dina & Ghaleb [21], and others have studied some aspects of the problem. Another technique, relying upon perturbation approaches are followed. Works by Cole [22] and Ghaleb & Hefni [23], Hanna et al. [24] have investigated the stationary case of the geophysical problem.

Numerical investigations such as those dealt with in [25] have been carried out. One can find a review of these numerical approaches in Yeung [26].

Most of the papers cited above deal with steady-state cases. These papers considered that the motion of the fluid remains for all times, and this is unnatural. In general, the steady-state problem has not a unique mathematical solution (see Stoker [27,28] for a discussion of this aspect). Many geophysical phenomena (such as the case considered by Abou-Dina [29] are transient, and their steady-state limit can never take place. These works did not consider the transient motions. Mathematically, to guarantee a unique solution, one should consider the initial conditions.

Following the shallow water theory, Abou-Dina & Helal [30–32] have considered the transient aspects of the problem, for various topographies.

The general problem of nonlinear transient fluid waves has been reduced by Abou-Dina and Helal [16,17] to a coupled set of integral and PDEs and they presented a numerical solution for their system. The stability of their procedure deteriorated at large time moments and needs careful examination. Hassan [18] has implemented the same idea proposed by Abou-Dina and Helal [16,17] and partially remedied this inconvenient result by using a different numerical procedure.

Abou-Dina [20] has developed a nonlinear theory of the nonstationary waves, resulting in following an initial shape of the fluid surface over a non-horizontal bottom. The problem was considered as an initial value problem. Also, Shroy et al. [33], Whitewell et al. [34], Marshal [35], and

Zhang [36] have considered the phenomenon of wave propagation within the nonlinear theory of motion.

Germain [37] has discussed the limitations on the geometry of the problem assumed to be satisfied in the shallow water theory. These limitations were considered by Abou-Dina and Helal [30,31] in the applications. In contrast to this, the approach proposed by Abou-Dina [22] is free from these limitations and it only requires a small vertical extent of the shape of the bottom. Besides, Chen et al. [38], Marshal [35], Spall [39] and Soontiens [40] have dealt with the fluid flow over irregular topographies and discovered the impact of the shape of the bottom on the propagation of waves.

Moreover, Nonlinear topographies in the vast ocean play a pivotal role in shaping the dynamics of ocean currents and the distribution of marine life. The complex interplay between the ocean's bottom topography and the fluid dynamics above creates a rich tapestry of mesoscale circulation patterns. Ahmad et. al [41] has discussed the stochastic solitons of short wave intermediate dispersive variable equations. Gao has investigated many important nonlinear physical phenomena like two-layer liquid and elastic waves [42], oceanic shallow water on generalized Whitham–Broer–Kaup–Boussinesq–Kupershmidt system [43], wave processes in acoustics, hydrodynamics and oceanography by means of an extended coupled (2+1)-dimensional Burgers system [44]. Gao et. al [45] has investigated the solitons for Ablowitz-Ladik equation and generalized Darboux transformation. Similar work on the physical implications of nonlinear theory was investigated by [46-49].

In this work, we examine the gravity waves, in oceans with irregular topography, generated by the effect of winds blowing on the free surface. Similar subjects attract the attention of several authors from both experimental or theoretical points of view (Bertin et al. [50], Markina et al. [51] and references included therein). A suitable mathematical model simulating the considered phenomenon is formulated. We formulated the equations of the problem via the velocity potential. A classical perturbation technique, in powers of a parameter identifying the applied external pressure (simulating the blowing winds) and the geometry of the topography, is introduced to handle this nonlinear system. Linear and nonlinear theories are formulated, and the procedure for obtaining higher-order theories is indicated. The proposed mathematical procedure relies upon the use of the joint complex Fourier and Laplace transforms (Tranter [52]). According to the limitations assumed on the proposed model, it is found that the bottom corrugation is irrelevant to the solution of the linear theory, and this is similar to the results of Abou-Dina [20].

Here, the necessity for the nonlinear theory in predicting the considered phenomenon is discussed. The nonlinear expressions for the potential, the free surface's height, and the stream function are calculated. The quadratic solution according to the nonlinear theory technique depends explicitly on the shape of the bottom. The contribution of the bottom's shape to the free surface form could be isolated and presented explicitly. This check is made by carrying out a comparison between the lowest streamline and the trace of the topography. A good and satisfactory agreement between these two curves is obtained.

There is a very limited number of published works that worked on this mode, you can see Alaidrous [10], Abou-Dina [20] and our new achievement is that we will present an approach to obtain quadratic solutions from nonlinear theory technique. We describe how changing some of the phenomenon's characteristics affects the waves that are produced. More specifically, the effects of increasing the frequency of the applied external pressure, increasing the area exposed to the external pressure, and studying fluctuations over time on the propagation of created waves are explored. The reliability of the proposed solution is examined through a certain worked application.

2. The mathematical model

The mathematical model simulating the considered phenomenon consists of a homogeneous and ideal layer of the fluid, occupying an open channel with a non-horizontal bottom (Figure 1). An outer pressure is applied to the fluid's surface. This pressure generates waves propagating, in the fluid, towards both extremities of the channel. Specifying the externally applied pressure (simulating the winds), we require to describe the fluid at every instant of time.

The problem is studied in two dimensions and the vertical height of the topography is assumed small compared with the other dimensions. The coordinate system $O(x, y)$, of Figure 1 is used. The origin "O" lies the free surface's mean level, the $x-$axis is horizontal and the $y-$axis is vertical.

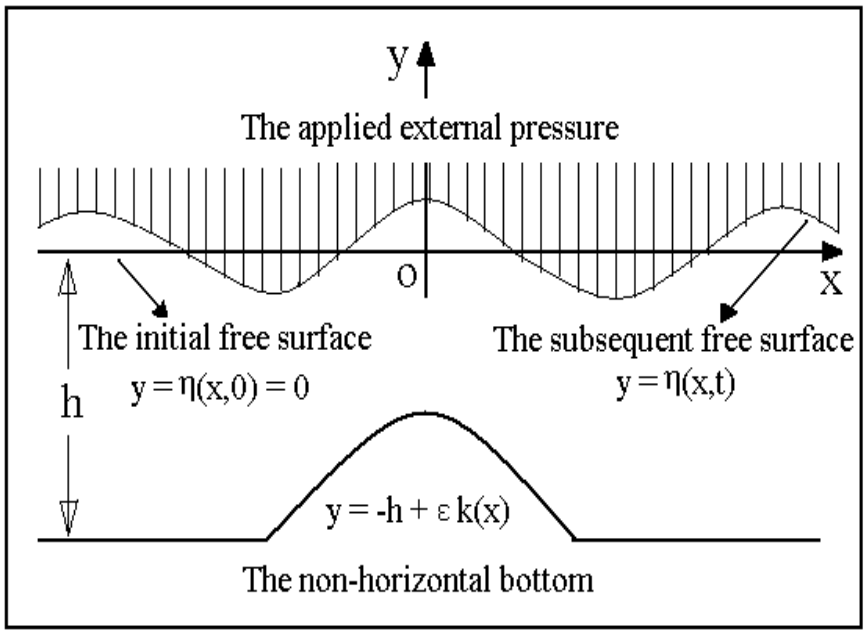

Figure 1. The graphical model of the mathematical Problem and its frame of reference.

3. Equations and conditions

The external pressure acting on the fluid's surface is regular, and the motion starts from rest. This is sufficient for the subsequent motion of the fluid to be non-rotational ($\vec{\nabla} \times \vec{V} = 0, \vec{V}$ is the velocity vector) (Lamb [19]). The problem is now to determine a scalar potential $\Phi(x, y, t)$ (with $\vec{V} = \vec{\nabla}\Phi(x, y, t)$), together with the shape of the surface $\eta(x, t)$. These unknown functions satisfy the following system (Lamb [19] and Stoker [28]).

(I) In the fluid mass, the following condition must be satisfied:

$$\nabla^2\Phi = 0, -h + \varepsilon k(x) \leq y \leq \eta(x, t), |x| < \infty, \tag{1}$$

where ∇^2 denotes the Laplacian operator: $\nabla^2 = \frac{\partial^2}{\partial x^2} + \frac{\partial^2}{\partial y^2}$.

The pressure is given as:

$$P(x, y) = \rho\left\{\frac{\partial}{\partial t}\Phi + \frac{1}{2}\left[\left(\frac{\partial}{\partial x}\Phi\right)^2 + \left(\frac{\partial}{\partial y}\Phi\right)^2\right] + gy\right\}, \tag{2}$$

where ρ is the fluid's density.
(II) On $y = \eta(x,t)$, the impermeability implies:

$$\frac{\partial}{\partial y}\Phi = \frac{\partial \eta}{\partial t} + \frac{\partial \eta}{\partial x}\frac{\partial}{\partial x}\Phi \quad at \quad y = \eta(x,t). \tag{3}$$

The pressure on this boundary is prescribed at every instant of time. This condition is expressed as:

$$\frac{\partial}{\partial t}\Phi + \frac{1}{2}\left[\left(\vec{\nabla}\Phi\right)^2\right] + gy + \varepsilon P_0(x,t) = 0 \ \ at \ \ y = \eta(x,t), \tag{4}$$

where P_0 is a given function of its variables characterizing the external pressure acting on the surface. The function $P_0(x,t)$ is assumed to vanish at $t = 0$ (i.e., $P_0(x,0) = 0$).
(III) The impermeability of the bottom implies:

$$\frac{\partial}{\partial y}\Phi - \varepsilon\frac{dk}{dx}\frac{\partial}{\partial x}\Phi = 0 \quad at \quad y = -h + \varepsilon k(x). \tag{5}$$

The function $k(x)$, characterizing the bottom topography, is continuously differentiable and ε is a small parameter.
(IV) The radiation condition at infinity is expressed as (Stoker [28]):

$$\lim_{|x|\to\infty}\Phi = 0, \ \lim_{|x|\to\infty}\frac{\partial}{\partial x}\Phi = 0. \tag{6}$$

(V) At $t = 0$, the conditions are expressed in the form:

$$\Phi = 0 \quad at \quad t = 0, \tag{7}$$

$$\frac{\partial}{\partial t}\Phi = 0 \quad at \quad t = 0, y = 0. \tag{8}$$

Conditions (3,4) are nonlinear conditions and applied on $y = \eta(x,t)$, and the function η is one of the unknowns of the system. The functions Φ and η are coupled in this system and it does not seem probable to uncouple these functions. Further, the domain of the problem does not seem to be bounded by coordinate curves in any system of coordinates. Because of these properties, it is not expected to seek the solution of the above system as a combination of elementary functions.

4. The perturbation technique

To overcome the difficulties, indicated earlier, we follow Abou-Dina [20] and use a perturbation procedure for solving. Following this method, the functions Φ and η are considered developable in the form (Nayfeh [53])

$$\Phi(x,y,t) = \sum_{n=1}^{\infty}\varepsilon^n\Phi_n(x,y,t), \ \eta(x,t) = \sum_{n=1}^{\infty}\varepsilon^n\eta_n(y,t), \tag{9}$$

and we suppose that the system of equations is verified for all orders of ε.

Nonlinear conditions (3,4) on $y = \eta(x,t)$ and condition (5) on $y = -h + \varepsilon k(x)$ are to be developed in powers of ε. The system of equations so obtained is called the perturbed system.

4.1. The linear theory

The linear theory arises when neglecting ε^n, $n > 1$, in the perturbed system. This theory is also called a first-order theory. According to this theory, the domain of the problem reduces to a uniform

strip of depth h, and it is required to seek $\Phi_1(x,y,t)$ defined in this strip (with $\Phi = \varepsilon\Phi_1$). This function satisfies the equations:
(*I.1*) In the domain of the problem:

$$\nabla^2\Phi_1 = 0, -\infty \le x < \infty, -h \le y \le 0. \tag{10}$$

(*II.1*) At $y = 0$:

$$\frac{\partial^2}{\partial t^2}\Phi_1 + g\frac{\partial}{\partial y}\Phi_1 = -\frac{\partial}{\partial t}P_0(x,t). \tag{11}$$

(*III.1*) At $y = -h$:

$$\frac{\partial}{\partial y}\Phi_1 = 0. \tag{12}$$

(*IV.1*) The radiation conditions:

$$\lim_{|x|\to\infty}\Phi_1 = 0, \ \lim_{|x|\to\infty}\frac{\partial}{\partial x}\Phi_1 = 0. \tag{13}$$

(*V.1*) At $t = 0$:

$$\Phi_1 = 0, \tag{14}$$

$$\frac{\partial}{\partial y}\Phi_1 = 0 \ \text{ at } \ y = 0. \tag{15}$$

The height of the surface is $\eta = \varepsilon\eta_1$, with

$$\eta_1(x,t) = -\frac{1}{g}\left[\frac{\partial}{\partial t}\Phi_1(x,y,t) + P_0(x,t)\right] \ \text{ at } \ y = 0. \tag{16}$$

4.2. The nonlinear (quadratic) theory

The nonlinear theory arises if we stop the perturbed system at the second order of ε. Here also, the problem is defined in the same horizontal strip, and it is required to determine Φ_2 (with $\Phi(x,y,t) = \varepsilon\Phi_1(x,y,t) + \varepsilon^2\Phi_2(x,y,t)$). This function satisfies the following equations:
(*I.2*) In the domain of the problem:

$$\nabla^2\Phi_1 = 0, -\infty \le x < \infty, -h \le y \le 0. \tag{17}$$

(*II.2*) At $y = 0$:

$$\frac{\partial^2}{\partial t^2}\Phi_2 + g\frac{\partial}{\partial y}\Phi_2 = F(x,t), \ y = 0, \tag{18}$$

with

$$F(x,t) = g\left[\frac{\partial}{\partial t}A(x,t) - B(x,t)\right], \tag{19}$$

where

$$A(x,t) = -\frac{1}{g}\left[\frac{1}{2}\left(\frac{\partial\Phi_1}{\partial x}\right)^2 + \frac{1}{2}\left(\frac{\partial\eta_1}{\partial t}\right)^2 + \eta_1.\frac{\partial^2\eta_1}{\partial t^2}\right]_{y=0}, \tag{20}$$

$$B(x,t) = -\frac{\partial}{\partial x}\left[\eta_1 . \frac{\partial}{\partial x}\Phi_1\right]_{y=0}. \tag{21}$$

(*III.2*) At $y = -h$:

$$\frac{\partial}{\partial y}\Phi_2 = G(x,t),\ y = -h, \tag{22}$$

with

$$G(x,t) = \frac{\partial}{\partial x}\left[k(x).\frac{\partial \Phi_1}{\partial x}\right],\ y = -h. \tag{23}$$

(*IV.2*) The radiation conditions:

$$\lim_{|x|\to\infty} \Phi_2 = 0,\ \lim_{|x|\to\infty} \frac{\partial}{\partial x}\Phi_2 = 0. \tag{24}$$

(*V.2*) At $t = 0$:

$$\Phi_2 = 0,\ \text{at}\ \ t = 0, \tag{25}$$

$$\frac{\partial}{\partial y}\Phi_2 = 0\ \text{at}\ \ t = 0, y = 0. \tag{26}$$

The second-order expression of η writes $\eta(x,t) = \varepsilon\eta_1(x,t) + \varepsilon^2\eta_2(x,t)$, with

$$\eta_2(x,t) = -\frac{1}{g}\frac{\partial}{\partial t}\Phi_2(x,y,t) + A(x,t),\ \text{at}\ \ y = 0. \tag{27}$$

The system of equations for any other order higher than the second can be formulated in the same way.

4.3. Solution of the problem

To obtain solutions for these theories, we follow Abou-Dina [20] and use the technique of integral transforms. The functions of Φ and η are thus assumed to possess complex Fourier transforms (Lighthill [54]). We denote by $\tilde{A}(\zeta)$ the complex Fourier transform of A(x) (Tranter [52]). Hence,

$$\tilde{A}(\zeta) = \int_{-\infty}^{\infty} A(x,t)e^{i\zeta x}dx\,, -\infty < \zeta < \infty. \tag{28}$$

We write $\bar{B}(s)$ for the Laplace transform of the function $B(t)$ (Tranter [43]). Therefore:

$$\bar{B}(s) = \int_0^{\infty} B(t)e^{-st}dt\,,\ s \geq 0. \tag{29}$$

By $\bar{\tilde{C}}(\zeta, s)$, we mean the joint complex Fourier and Laplace transform of the function C. For the solution of the theorems formulated above, we use the joint complex Fourier and Laplace transforms with their inversion formulae, see Abou-Dina [20] for similar calculations.

4.4. Solution of the linear theory

For the first order (10)−(15), the solution is obtained as:

$$\Phi_1(x,y,t) = -\frac{1}{2\pi}\int_{-\infty}^{\infty}\left[\frac{\cosh(\zeta(y+h))}{\cosh(\zeta h)}\int_0^t \cos(\omega(t-t').\widetilde{P_0}(\zeta,t')dt'\right]e^{-i\zeta x}d\zeta, \tag{30}$$

$$\text{with } \omega^2(\zeta) = g\zeta\tanh(\zeta h). \tag{31}$$

The function η_1 is given, by (16) and (31), as:

$$\eta_1(x,t) = -\frac{1}{2\pi g}\int_{-\infty}^{\infty}\omega\left[\int_0^t \cos(\omega(t-t').\widetilde{P_0}(\zeta,t')dt'\right]e^{-i\zeta x}d\zeta. \tag{32}$$

4.5. Solution of the second order (nonlinear) theory

The solution of the second order (nonlinear) theory (17)−(26), is obtained as:

$$\Phi_2(x,y,t) = \frac{1}{2\pi}\int_{-\infty}^{\infty}\left[\left(\frac{g\cosh(\zeta(y+h))}{\omega\cosh(\zeta h)}\right)\int_0^t\left\{\omega\tilde{A}(\zeta,t')\cos\omega(t-t') - \left(\tilde{B}(\zeta,t') + \frac{\tilde{G}(\zeta,t')}{\cosh(\zeta h)}\right)\sin\omega(t-t')\right\}dt' + \frac{\sinh(\zeta h)}{\zeta\cosh(\zeta h)}\tilde{G}(\zeta,t')\right]e^{-i\zeta x}d\zeta. \tag{33}$$

The function η_2 is given, by (27) and (33), as: $\eta_2(x,t) = \eta_{21}(x,t) + \eta_{22}(x,t)$, with

$$\eta_{21}(x,t) = \frac{1}{2\pi}\int_{-\infty}^{\infty}\left[\int_0^t\left\{\omega\tilde{A}(\zeta,t')\sin\omega(t-t') + \tilde{B}(\zeta,t')\cos\omega(t-t')\right\}dt'\right]e^{-i\zeta x}d\zeta, \tag{34}$$

$$\eta_{22}(x,t) = \frac{1}{2\pi}\int_{-\infty}^{\infty}\left[\frac{1}{\cosh(\zeta h)}\int_0^t\tilde{G}(\zeta,t')\cos\omega(t-t')\,dt'\right]e^{-i\zeta x}d\zeta. \tag{35}$$

In contrast with the results of the linear theory, one notes the influence of the bottom shape, in the results of the second order (nonlinear) theory, represented in the function $G(x,t)$ given by (23) depending on the function $k(x)$ describing the bottom topography.

5. **The quadratic (nonlinear) solution**

The solutions of the first and second-order theories, given above, lead to the following expressions:

5.1. The function $\Phi(x,y,t)$

Relations (30) and (33) give the potential ($\Phi(x,y,t) = \Phi_1(x,y,t) + \varepsilon^2\Phi_2(x,y,t)$) as

$$\Phi(x,y,t) = \frac{1}{2\pi}\int_{-\infty}^{\infty}\left[\left(\frac{\cosh(\zeta(y+h))}{\omega\cosh(\zeta h)}\right)\text{ x }\int_0^t\left\{\varepsilon\widetilde{P_0}(\zeta,t').\cos\omega(t-t') - \varepsilon^2\frac{g}{\omega}\left(\omega\tilde{A}(\zeta,t')\cos\omega(t-t') - \left[\tilde{B}(\zeta,t') + \frac{\tilde{G}(\zeta,t')}{\cosh(\zeta h)}\right]\sin\omega(t-t')\right)\right\}dt' - \varepsilon^2\frac{\sinh(\zeta h)}{\zeta\cosh(\zeta h)}\tilde{G}(\zeta,t')\right]e^{-i\zeta x}d\zeta. \tag{30}$$

5.2. The function Ψ

The Cauchy-Riemann conditions ($\frac{\partial}{\partial x}\Phi = \frac{\partial}{\partial y}\Psi, \frac{\partial}{\partial y}\Phi = -\frac{\partial}{\partial x}\Psi$) give the relations between the functions Ψ and Φ. Using (36) together with these relations, we obtain the quadratic expression of Ψ as $\Psi(x,y,t) = \varepsilon\Psi_1(x,y,t) + \varepsilon^2\Psi_{21}(x,y,t) + \varepsilon^2\Psi_{22}(x,y,t)$, with:

$$\Psi_1(x,y,t) = \frac{i}{2\pi}\int_{-\infty}^{\infty} e^{-i\zeta x}\alpha(\zeta,t)\sinh\big(\zeta(y+h)\big)\,d\zeta, \tag{37}$$

and

$$\Psi_{21}(x,y,t) = \frac{i}{2\pi}\int_{-\infty}^{\infty} e^{-i\zeta x}\beta(\zeta,t)\sinh\big(\zeta(y+h)\big)\,d\zeta, \tag{38}$$

with

$$\Psi_{22}(x,y,t) = \frac{i}{2\pi}\int_{-\infty}^{\infty} e^{-i\zeta x}\gamma(\zeta,t)\cosh(\zeta y)\,d\zeta, \tag{39}$$

with

$$\alpha(\zeta,t) = \frac{1}{\cosh(\zeta y)}\alpha_c(\zeta,t). \tag{40}$$

$$\beta(\zeta,t) = \frac{-g}{2\pi\omega\cosh(\zeta h)}\int_{-\infty}^{\infty}\Big[\int_0^t\Big\{\frac{\omega}{g}\Big\{\frac{1}{2}\Big(\xi(\zeta-\xi) - \frac{\varphi^2\theta^2}{g^2}\Big)\alpha_c(\zeta,t')\alpha_c(\zeta-\xi,t') - \frac{\varphi^2\theta}{g^2}\Big(\widetilde{P_0}(\zeta,t') - \varphi\alpha_s(\zeta,t')\Big)\alpha_s(\zeta-\xi,t')\Big\}\cos\omega(t-t') - \Big(\frac{\zeta\xi\theta}{g}\alpha_c(\zeta,t')\alpha_s(\zeta-\xi,t') + \frac{\zeta\xi}{\cosh(\zeta h)\cosh(\xi h)}\alpha_c(\zeta,t').\tilde{k}(\zeta-\xi)\Big)\sin\omega(t-t')\Big\}dt'\Big]d\xi, \tag{41}$$

and

$$\gamma(\zeta,t) = \frac{-1}{2\pi\cosh(\zeta h)}\int_{-\infty}^{\infty}\frac{\xi}{\cosh(\zeta h)}\alpha_c(\xi,t).\tilde{k}(\zeta-\xi)d\xi, \tag{42}$$

where the functions α_c and α_s are given in terms of ζ, t as:

$$\alpha_c(\zeta,t) = \int_0^t \widetilde{P_0}(\zeta,t').\cos\omega(t-t')\,dt', \tag{43}$$

$$\alpha_s(\zeta,t) = \int_0^t \widetilde{P_0}(\zeta,t').\sin\omega(t-t')\,dt', \tag{44}$$

where $\omega(\zeta)$ is given in (31), and φ and θ are given as:

$$\varphi^2 = g\xi\tanh(\xi h), \tag{45}$$

and

$$\theta^2 = g(\zeta-\xi)\tanh(\zeta-\xi)h. \tag{46}$$

5.3. The function $\eta(x,t)$

Using (32), (34) and (35), we obtain the quadratic height of the free surface as

$$\eta(x,t)=\frac{1}{2\pi}\int_{-\infty}^{\infty}[\varepsilon\tilde{\eta}_1(\zeta,t)+\varepsilon^2\tilde{\eta}_{21}(\zeta,t)+\varepsilon^2\tilde{\eta}_{22}(\zeta,t)]e^{-i\zeta x}d\zeta, \tag{47}$$

with

$$\tilde{\eta}_1(\zeta,t)=-\frac{\omega}{g}\alpha_s(\zeta,t). \tag{48}$$

$$\tilde{\eta}_{21}(\zeta,t)=\frac{1}{2\pi g}\int_{-\infty}^{\infty}\Big[\int_0^t\Big\{\omega\Big\{\frac{1}{2}\Big(\xi(\zeta-\xi)-\frac{\varphi^2\theta^2}{g^2}\Big)\alpha_c(\zeta,t')\alpha_c(\zeta-\xi,t')-\frac{\varphi^2\theta}{g^2}\Big(\widetilde{P_0}(\zeta,t')-$$

$$\varphi\alpha_s(\zeta,t')\Big)\alpha_s(\zeta-\xi,t')\Big\}\sin\omega(t-t')+\zeta\xi\theta\alpha_c(\zeta,t')\alpha_s(\zeta-\xi,t')\cos\omega(t-t')\Big\}dt'\Big]d\xi. \tag{49}$$

$$\tilde{\eta}_{22}(\zeta,t)=\frac{1}{2\pi}\int_{-\infty}^{\infty}\frac{\zeta\xi\tilde{k}(\zeta-\xi)}{\cosh(\zeta h)\cosh(\xi h)}\Big(\int_0^t\alpha_c(\zeta,t')\cos\omega(t-t')\,dt'dt'\Big)d\xi. \tag{50}$$

We denote by $\eta_h(x,t)$, the elevation of the free surface for a horizontal bottom. This function takes the form:

$$\eta_h(x,t)=\varepsilon\eta_1(x,t)+\varepsilon^2\eta_{21}(x,t)=\frac{1}{2\pi}\int_{-\infty}^{\infty}e^{-i\zeta x}[\varepsilon\tilde{\eta}_1(\zeta,t)+\varepsilon^2\tilde{\eta}_{21}(\zeta,t)]d\zeta. \tag{51}$$

6. The validity of the solution

In the present section, we carry out a numerical study to check the validity of the solution obtained above. We consider the particular case where the applied external pressure function $P_0(x,t)$ has finite supports of the following form:

$$P_0(x,t)=\begin{cases}\sin(\alpha_0 t), & \text{for } |x|\le a;\\ 0, & \text{for } |x|>a.\end{cases} \tag{52}$$

The topography of the bottom will be assumed to consist of an asymmetric hump of height $c=\varepsilon\bar{c}$ and width $2d$. The bottom is otherwise horizontal without corrugations. For this bottom, the function $k(x)$ is:

$$k(x)=\frac{\bar{c}}{2}\Big\{1+\cos\Big(\frac{\pi x}{d}\Big)\Big\}\{H(x+d)-H(x-d)\}, \tag{53}$$

whose Fourier transform takes the form:

$$\tilde{k}(\zeta)=\frac{\pi^2\bar{c}\sin(\zeta d)}{\zeta(\pi^2-\zeta^2d^2)}. \tag{53}$$

For such a choice, the functions α, β, and γ intervening in the expression of $\Psi(x,y,t)$ take the following forms:

$$\alpha(\zeta,t)=\frac{2\alpha_0\sin(\zeta a)}{\zeta\cosh(\zeta h)}.\left(\frac{\cos(\alpha_0 t)-\cos(\omega t)}{\omega^2-\alpha_0^2}\right). \tag{54}$$

$$\beta(\zeta,t)=\frac{1}{\cosh(\zeta h)}.\int_{-\infty}^{\infty}\frac{\sin(\zeta a)}{(\zeta-\xi)}\left[\frac{\sin((\zeta-\xi)a)}{(\varphi^2-\alpha_0^2)(\theta^2-\alpha_0^2)}\left(\beta_1(\zeta,\xi,t)+\beta_2(\zeta,\xi,t)\right)+\beta_3(\zeta,\xi,t)\right]d\xi, \tag{55}$$

and

$$\gamma(\zeta,t)=\frac{-\alpha_0\bar{c}\pi}{\cosh(\zeta h)}.\int_{-\infty}^{\infty}\frac{\sin(\zeta a)\sin((\zeta-\xi)d)}{(\zeta-\xi)(\pi^2-(\zeta-\xi)^2d^2)\cosh(\zeta h)}.\left(\frac{\cos(\alpha_0 t)-\cos(\varphi t)}{\varphi^2-\alpha_0^2}\right)d\xi, \tag{57}$$

where

$$\beta_1(\zeta,\xi,t)=\frac{\alpha_0^2}{2\pi}\left\{\left[(\zeta-\xi)+\frac{\varphi^2\theta^2}{\xi g^2}\right]\left(\frac{\sin(\omega t)}{\omega}\right)+\left[(\zeta-\xi)-3\frac{\varphi^2\theta^2}{\xi g^2}\right]\left(\frac{2\alpha_0\sin(2\alpha_0 t)-\omega\sin(\omega t)}{(2\alpha_0)^2-\omega^2}\right)-\right.$$
$$\left[(\zeta-\xi)-3\frac{\varphi^2\theta(\theta+2\alpha_0)}{\xi g^2}\right]\left(\frac{(\alpha_0+\theta)\sin((\alpha_0+\theta)t)-\omega\sin(\omega t)}{(\alpha_0+\theta)^2-\omega^2}\right)-\left[(\zeta-\xi)-\right.$$
$$\left.\frac{\varphi^2\theta(\theta-2\alpha_0)}{\xi g^2}\right]\left(\frac{(\alpha_0-\theta)\sin((\alpha_0-\theta)t)-\omega\sin(\omega t)}{(\alpha_0-\theta)^2-\omega^2}\right)-\left[(\zeta-\xi)-\frac{\varphi^2\theta^2(\alpha_0+2\varphi)}{\alpha_0\xi g^2}\right]\left(\frac{(\alpha_0+\varphi)\sin((\alpha_0+\varphi)t)-\omega\sin(\omega t)}{(\alpha_0+\varphi)^2-\omega^2}\right)-$$
$$\left[(\zeta-\xi)-\frac{\varphi^2\theta^2(\alpha_0-2\varphi)}{\alpha_0\xi g^2}\right]\left(\frac{(\alpha_0-\varphi)\sin((\alpha_0-\varphi)t)-\omega\sin(\omega t)}{(\alpha_0-\varphi)^2-\omega^2}\right)+\left[(\zeta-\xi)-\right.$$
$$\left.\frac{\varphi^2\theta(\theta+2\varphi)}{\xi g^2}\right]\left(\frac{(\varphi+\theta)\sin((\varphi+\theta)t)-\omega\sin(\omega t)}{(\varphi+\theta)^2-\omega^2}\right)+\left[(\zeta-\xi)-\frac{\varphi^2\theta(\theta-2\varphi)}{\xi g^2}\right]\left(\frac{(\varphi-\theta)\sin((\varphi-\theta)t)-\omega\sin(\omega t)}{(\varphi-\theta)^2-\omega^2}\right)\Big\}. \tag{58}$$

$$\beta_2(\zeta,\xi,t)=\frac{-\alpha_0\zeta\theta}{\pi\omega}\left\{\theta\left[\left(\frac{2\alpha_0\sin(\omega t)-\omega\sin(2\alpha_0 t)}{(2\alpha_0)^2-\omega^2}\right)-\left(\frac{(\alpha_0+\varphi)\sin(\omega t)-\omega\sin((\alpha_0+\varphi)t)}{(\alpha_0+\varphi)^2-\omega^2}\right)+\right.\right.$$
$$\left.\left(\frac{(\alpha_0-\varphi)\sin(\omega t)-\omega\sin((\alpha_0-\varphi)t)}{(\alpha_0-\varphi)^2-\omega^2}\right)\right]-\alpha_0\left[\left(\frac{(\theta+\alpha_0)\sin(\omega t)-\omega\sin((\theta+\alpha_0)t)}{(\theta+\alpha_0)^2-\omega^2}+\frac{(\theta-\alpha_0)\sin(\omega t)-\omega\sin((\theta-\alpha_0)t)}{(\theta-\alpha_0)^2-\omega^2}\right)-\right.$$
$$\left.\left.\left(\frac{(\theta+\varphi)\sin(\omega t)-\omega\sin((\theta+\varphi)t)}{(\theta+\varphi)^2-\omega^2}+\frac{(\theta-\varphi)\sin(\omega t)-\omega\sin((\theta-\varphi)t)}{(\theta-\varphi)^2-\omega^2}\right)\right]\right\}, \tag{59}$$

and

$$\beta_3(\zeta,\xi,t)=\frac{-\alpha_0\bar{c}\pi g\zeta\sin((\zeta-\xi)d)}{\cosh(\xi h)\cosh(\zeta h)(\pi^2-(\zeta-\xi)^2d^2)}\times\left(\frac{\cos(\omega t)}{(\alpha_0^2-\omega^2)(\varphi^2-\omega^2)}-\frac{\cos(\alpha_0 t)}{(\alpha_0^2-\omega^2)(\varphi^2-\alpha_0^2)}+\frac{\cos(\varphi t)}{(\varphi^2-\omega^2)(\varphi^2-\alpha_0^2)}\right). \tag{60}$$

The stream function is obtained in the vicinity of the topography by setting $y=-h+\varepsilon\sigma(x)$ in $\Psi(x,y,t)$, then,

$$\Psi(x,y,t)=\varepsilon\Psi_1(x,-h+\varepsilon\sigma(x),t)+\varepsilon^2\Psi_{21}(x,-h+\varepsilon\sigma(x),t)+\varepsilon^2\Psi_{22}(x,-h+\varepsilon\sigma(x),t). \tag{61}$$

Expressing these functions in powers of σ one gets:

$$\Psi(x,y,t)=\varepsilon\sigma\frac{\partial\Psi_1}{\partial y}(x,-h,t)+\varepsilon^2\Psi_{22}(x,-h,t)+O(\varepsilon^3). \tag{62}$$

Here, Ψ_1 and Ψ_{22} are given by (37), (39, (42).

The streamlines of this flow are given as the solution of the algebraic equation:

$$\Psi(x,y,t)=C_s. \tag{63}$$

Each streamline is distinguished by a constant real value given to the parameter C_s. The single-valued function $\Psi(x,y,t)$ given by (61), may be replaced by (62), for regions near the topography.

The calculated lowest streamline coincides with the topography if the obtained solution is the analytic solution. A comparison of this streamline with the topography can examine the validity of the proposed solution. We carry out this comparison using the choice, explained above, for the applied external pressure (52) and the bottom topography (53).

The parameter C_s takes the value C_b along the bottom. This value is obtained from (62) by putting $x = x_0$ and $\sigma = 0$, as:

$$C_b = \varepsilon^2 \Psi_{22}(x_0, -h, t), \tag{64}$$

where x_0 is chosen such that, the point $(x_0, -h)$ belongs to the flat part of the bottom. The streamline containing this point is the lowest one.

The equation of the lowest streamline ($y = -h + \varepsilon\sigma(x)$) is given by (62)–(64) as:

$$y = -h + \varepsilon \left[\frac{\Psi_{22}(x_0,-h,t) - \Psi_{22}(x,-h,t)}{\frac{\partial \Psi_1}{\partial y}(x,-h,t)} \right] + O(\varepsilon^2), \tag{65}$$

where Ψ_1 and Ψ_{22} are given by (37), (39) and (42).

Figure 2 display a comparison between the topography of the bottom, represented by the broken line, and the lowest streamline, represented by the solid line, at time $t = 8\sqrt{h/g}$ for the same height $c = 0.5h$ of the sinusoidal obstacle and maximum width $2d$ with $d = 0.3h$, $0.5h$ and $0.7h$ respectively. The remaining parameters are given the values $a = h$ and $\alpha_0 = 2\sqrt{g/h}$.

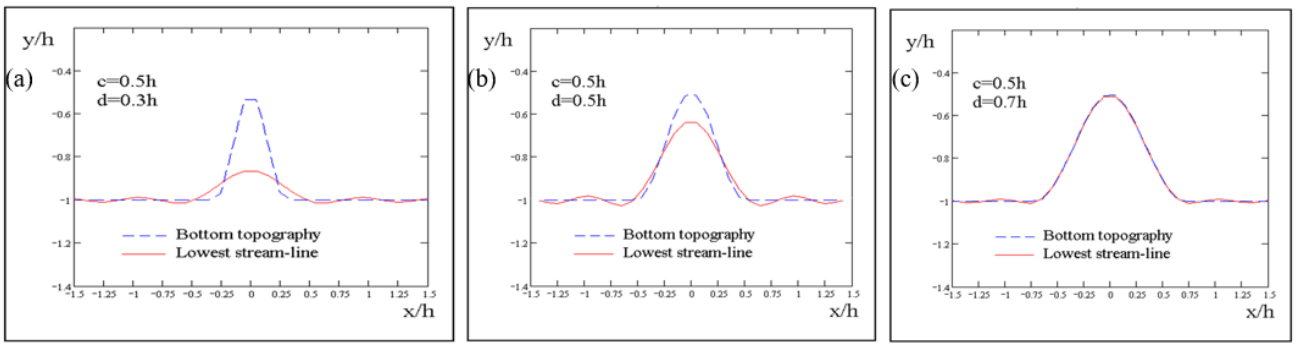

Figure 2. Comparison of the slope between the topography of the bottom and the lowest streamline for an obstacle with height ($c = 0.5h$) and width (d) at a time (t= $8\sqrt{h/g}$): (a) $d = 0.3h$; (b) $d = 0.5h$; (c) $d = 0.7h$.

These numerical experiments indicate that the slope of the topography plays the principal rule in the validity of the proposed solution and that the considered model is adequate and has a vast range of applicability for describing the propagation of waves over topographies, which have moderate and not very strong slopes. For topographies with sharp slopes, theories of orders higher than the second are therefore needed.

A comparison is also carried out at the same time $t = 5\sqrt{h/g}$ for three sinusoidal obstacles having the equal maximum width $2d$ with $d = h$ and different heights $c = 0.3h$, $0.6h$ and $0.9h$

respectively, with $a = h$ and $\alpha_0 = 2\sqrt{g/h}$. The results show a perfect coincidence between these two curves. This implies that, once the slope of the bottom is moderate, the accuracy of the solution which we propose has nothing to do with the effect of the height of the hump c/h.

7. **Necessity for the nonlinear theory in predicting the geophysical phenomenon**

Having studied and tested the validity of the approximate solution obtained earlier, we will investigate the effect of the nonlinear terms of the solution on the generation and propagation processes. Further, we will also use this solution to reveal and analyze some of the features of the oceanographic phenomenon under consideration.

We consider the particular choice used above, where the applied external pressure $P_0(x,t)$ and the bottom topography is given by (52) and (53). For such a choice, the quadratic form of the function $\eta(x,t)$ is given by (47), with:

$$\tilde{\eta}_1(\zeta,t) = -\frac{2\omega\sin(\zeta a)}{g\zeta}.\left(\frac{\omega\sin(\alpha_0 t)-\alpha_0\sin(\omega t)}{\omega^2-\alpha_0^2}\right). \tag{66}$$

$$\tilde{\eta}_{21}(\zeta,t) = \frac{1}{2\pi g}\int_{-\infty}^{\infty}\frac{\alpha_0^2\sin(\xi a)\sin((\zeta-\xi)a)}{(\zeta-\xi)(\varphi^2-\alpha_0^2)(\theta^2-\alpha_0^2)}\times\left[\left\{\omega^2\left[(\zeta-\xi)+\frac{\varphi^2\theta^2}{\xi g^2}\right]\left(\frac{1-\cos(\omega t)}{\omega^2}\right)+\left(\omega^2\left[(\zeta-\xi)-3\frac{\varphi^2\theta^2}{\xi g^2}\right]+4\zeta\theta^2\right)\left(\frac{\cos(\omega t)-\cos(2\alpha_0 t)}{(2\alpha_0)^2-\omega^2}\right)-\left(\omega^2\left[(\zeta-\xi)-\frac{\varphi^2\theta(\theta+2\alpha_0)}{\xi g^2}\right]+2\zeta\theta(\alpha_0+\theta)\right)\left(\frac{\cos(\omega t)-\cos((\alpha_0+\theta)t)}{(\alpha_0+\theta)^2-\omega^2}\right)-\left(\omega^2\left[(\zeta-\xi)-\frac{\varphi^2\theta(\theta-2\alpha_0)}{\xi g^2}\right]-2\zeta\theta(\alpha_0-\theta)\right)\left(\frac{\cos(\omega t)-\cos((\alpha_0-\theta)t)}{(\alpha_0-\theta)^2-\omega^2}\right)-\left(\omega^2\left[(\zeta-\xi)-\frac{\varphi^2\theta^2(\alpha_0+2\varphi)}{\alpha_0\xi g^2}\right]+\frac{2\zeta\theta^2(\alpha_0+\varphi)}{\alpha_0}\right)\left(\frac{\cos(\omega t)-\cos((\alpha_0+\varphi)t)}{(\alpha_0+\varphi)^2-\omega^2}\right)-\left(\omega^2\left[(\zeta-\xi)-\frac{\varphi^2\theta^2(\alpha_0-2\varphi)}{\alpha_0\xi g^2}\right]+\frac{2\zeta\theta^2(\alpha_0-\varphi)}{\alpha_0}\right)\left(\frac{\cos(\omega t)-\cos((\alpha_0-\varphi)t)}{(\alpha_0-\varphi)^2-\omega^2}\right)+\left(\omega^2\left[(\zeta-\xi)-\frac{\varphi^2\theta(\theta+2\varphi)}{\xi g^2}\right]+2\zeta\theta(\varphi+\theta)\right)\left(\frac{\cos(\omega t)-\cos((\varphi+\theta)t)}{(\varphi+\theta)^2-\omega^2}\right)+\left(\omega^2\left[(\zeta-\xi)-\frac{\varphi^2\theta(\theta-2\varphi)}{\xi g^2}\right]+2\zeta\theta(\varphi-\theta)\right)\left(\frac{\cos(\omega t)-\cos((\varphi-\theta)t)}{(\varphi-\theta)^2-\omega^2}\right)\right\}\right]d\xi, \tag{67}$$

and

$$\tilde{\eta}_{22}(\zeta,t) = \int_{-\infty}^{\infty}\frac{\pi\alpha_0\bar{c}\zeta\sin(\xi a)\sin((\zeta-\xi)d)}{\cosh(\zeta h)\cosh(\xi h)(\zeta-\xi)(\pi^2-(\zeta-\xi)^2d^2)}\times\left(\frac{\alpha_0\sin(\alpha_0 t)}{(\alpha_0^2-\omega^2)(\varphi^2-\alpha_0^2)}+\frac{\omega\sin(\omega t)}{(\alpha_0^2-\omega^2)(\omega^2-\varphi^2)}-\frac{\varphi\sin(\varphi t)}{(\alpha_0^2-\varphi^2)(\omega^2-\varphi^2)}\right)d\xi. \tag{68}$$

For a flat bottom, the free surface elevation for the present particular choice $\eta_h(x,t)$, reads:

$$\eta_h(x,t) = \varepsilon\eta_1(x,t)+\varepsilon^2\eta_{21}(x,t) = \frac{1}{2\pi}\int_{-\infty}^{\infty}[\varepsilon\tilde{\eta}_1(\zeta,t)+\varepsilon^2\tilde{\eta}_{21}(\zeta,t)]\,e^{i\zeta x}d\zeta. \tag{69}$$

The function $\eta(x,t)$, in the frame of the linear theory, takes the form:

$$\eta(x,t) = \frac{\varepsilon}{2\pi}\int_{-\infty}^{\infty}[\tilde{\eta}_1(\zeta,t)]\,e^{i\zeta x}d\zeta + O(\varepsilon^2). \tag{70}$$

7.1. Necessity for the quadratic (nonlinear) theory in the course of time

Figure 3 display the first order free surface elevation (dotted curves) and the quadratic free surface

elevation (solid curves) at the instants $T = 2\sqrt{h/g}$, $3\sqrt{h/g}$, $4\sqrt{h/g}$, and $5\sqrt{h/g}$, following the start of the motion. The remaining parameters are taken as $a = 2h$, $c = 0.4h$, $d = 3.0h$, $\alpha_0 = \sqrt{g/h}$ and $\varepsilon = 0.5$. These numerical experiments show that, although the linear theory may be adequate for describing the phenomenon in a small-time interval following the initial instant ($0 \leq T \leq 2\sqrt{h/g}$), the quadratic theory is indispensable for predicting the phenomenon as time elapses. The figures show also that the waves calculated by the nonlinear theory are faster than those calculated according to the linear one. The first-order theory screens important fluctuations of the free surface, characterizing the nonlinear features of the flow (cf. Figure 3(d)).

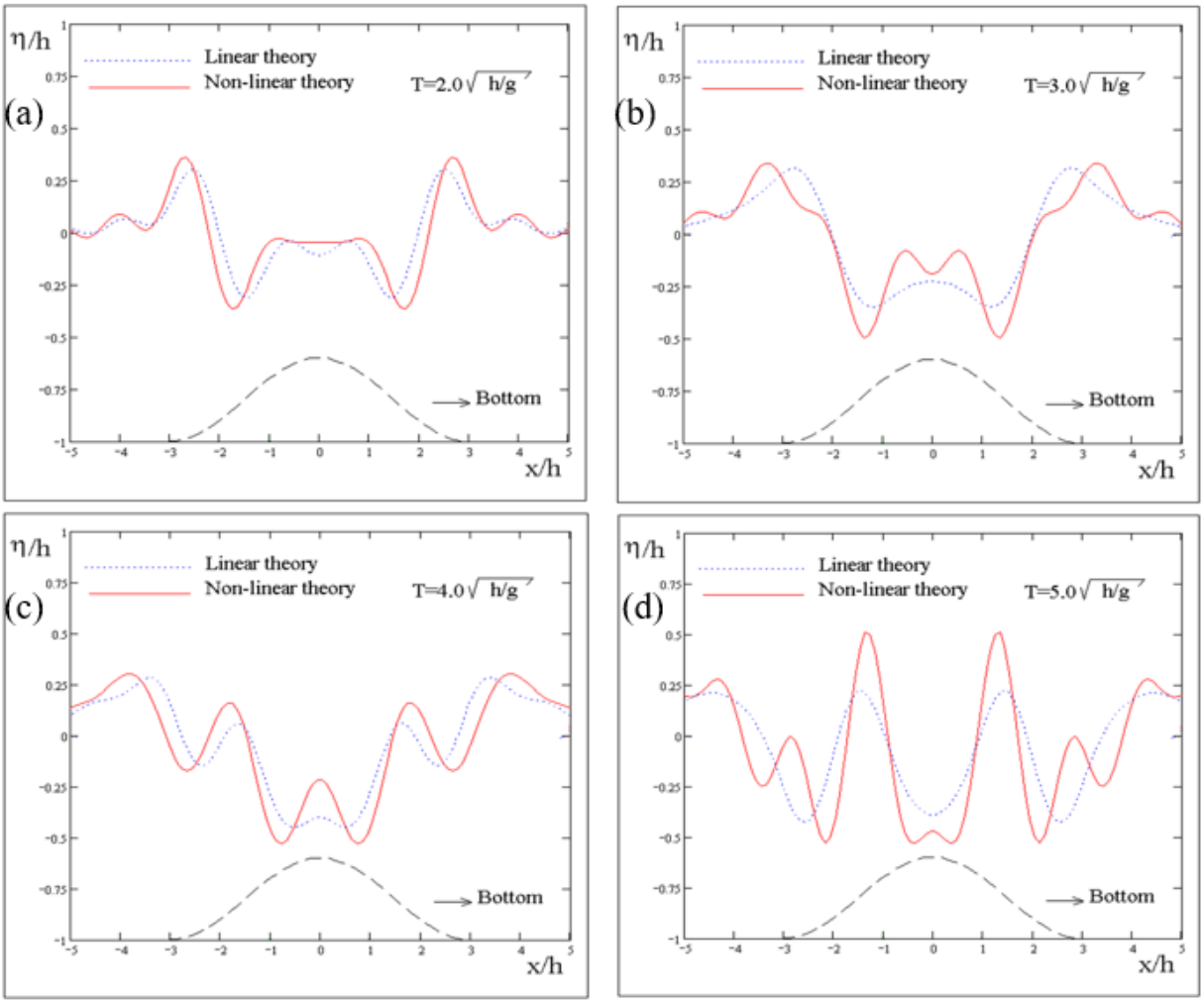

Figure 3. Comparison of the waves and the fluctuations on the free surface between the linear and nonlinear theories at a time T: (a) $T = 2.0\sqrt{h/g}$; (b) $T = 3.0\sqrt{h/g}$; (c) $T = 4.0\sqrt{h/g}$; (d) $T = 5.0\sqrt{h/g}$.

7.2. Necessity for the quadratic (nonlinear) theory with the increase of the frequency

Figure 4 exhibit a comparison between the free surface profile as predicted by the linear theory (dotted curves) and the free surface profile as predicted by the quadratic theory (solid curves) for the particular values of the frequencies: $\alpha_0 = 0.2\sqrt{g/h}$, $0.4\sqrt{g/h}$, $0.6\sqrt{g/h}$, and $0.8\sqrt{g/h}$,

respectively. The particular values given to the remaining parameters are $a = 2h$, $c = 0.3h$, $d = 5.0h$, $T = \sqrt{h/g}$, and $\varepsilon = 0.5$. These figures show that the linear theory is sufficient to describe the phenomenon only in the cases of low frequencies (cf. Figure 4(a)). The necessity for the quadratic theory increases with the increase of the frequency since the divergence between the linear and the quadratic theories increases with the increase of α_0. Here also, we note that the first-order theory cannot predict important fluctuations and slows the propagation of waves.

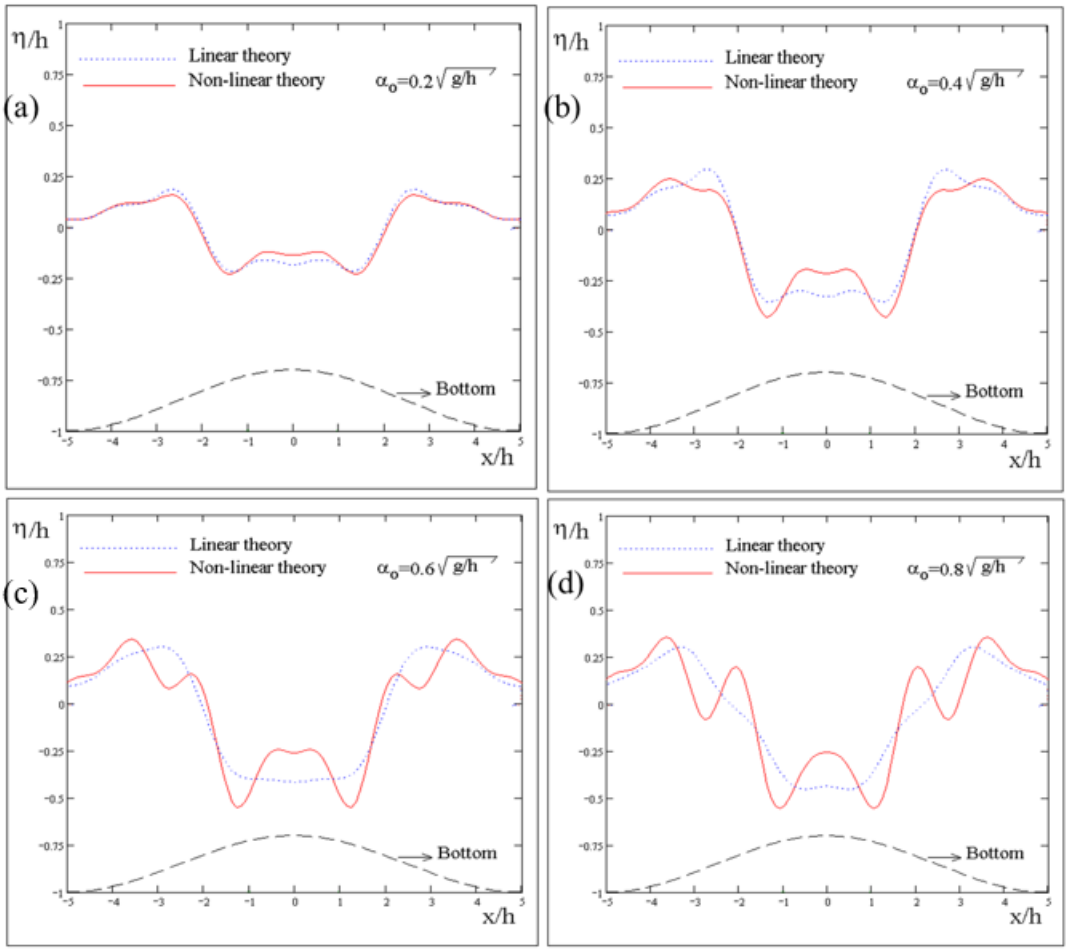

Figure 4. Comparison of the phenomenon of the free surface between the linear and nonlinear theories for the frequency α_0: (a) $\alpha_0 = 0.2\sqrt{g/h}$; (b) $\alpha_0 = 0.4\sqrt{g/h}$; (c) $\alpha_0 = 0.6\sqrt{g/h}$; (d) $\alpha_0 = 0.8\sqrt{g/h}$.

7.3. Necessity for the quadratic (nonlinear) theory with the increase of the area exposed to the blowing winds

Figure 5 present the free surface elevations as predicted by both the linear theory (dotted curves) and the nonlinear theory (solid curves) for several values of the parameter a representing half the area of the free surface, exposed to the applied external pressure, precisely for the values: $a = 2.0h$, $4.0h$, and $6.0h$. The particular values given to the remaining parameters are $c = 0.4h$, $d = 7.0h$, $\alpha_0 = \sqrt{g/h}$, $T = 4.0\sqrt{h/g}$ and $\varepsilon = 0.5$.

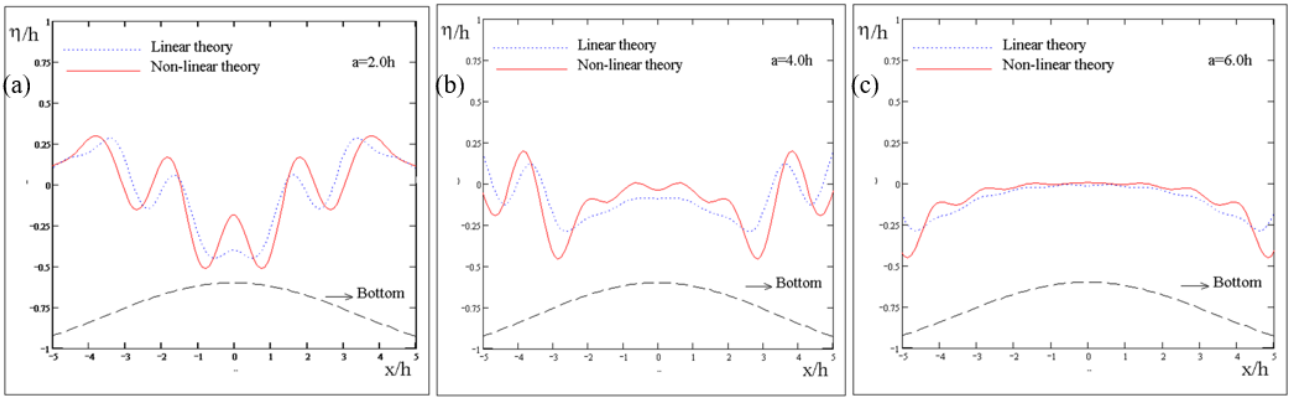

Figure 5. Comparison of the free surface elevations between the linear and nonlinear theories for half the area of the free surface a: (a) $a = 2.0h$; (b) $a = 4.0h$; (c) $a = 6.0h$.

These numerical experiments show that for small areas exposed to the blowing winds the nonlinear theory is necessary to predict the flow all-over the channel (cf. Figure 5(a)). For vast areas, exposed to the external pressure, the free surface just above the corrugated part of the bottom lies in the neighborhood of its position at rest and the outputs of two theories are too near from each other while far from this area, a significant difference between the outputs of the two theories appears and the necessity to the quadratic (nonlinear) theory arises.

8. Features of the oceanographic phenomenon

We make use of the results of the numerical experiments carried out in the frame of the preceding parts to pull some of the features of the oceanographic phenomenon of the waves, generated in oceans as a response to the winds blowing on their free surfaces. The application used in the present study is again the one considered above, where the external pressure is taken oscillatory, symmetrical, and uniform on a finite area of the free surface and vanishes otherwise. The bottom is horizontal with a sinusoidal symmetrical hump.

8.1. Variations occurring in the course of time

Figure 6 displays the profiles of the free surface calculated according to the nonlinear theory at the instants of time $T = 2\sqrt{h/g}$, $3\sqrt{h/g}$, $4\sqrt{h/g}$, and $5\sqrt{h/g}$, following the start of the motion, for the same particular values of the other parameters as those for Figures 2−5. The figure shows that, in the course of time, the free surface waves increase notably in amplitude and slightly in wavelength. This figure shows also that waves, generated on each side of the hump, advance slowly towards the corresponding extremity of the channel.

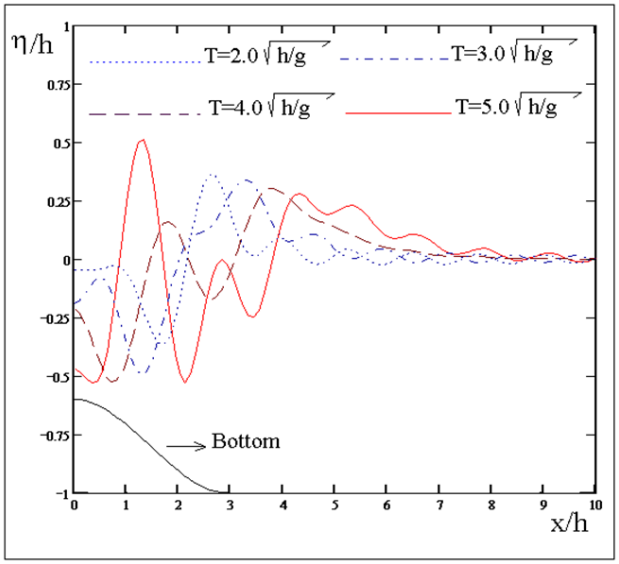

Figure 6. The profiles of the free surface waves of the nonlinear theory that is increase in amplitude, wavelength and other topography in the course of time.

8.2. Effect of the increase of the frequency

Figure 7 exhibits the free surface elevations calculated according to the nonlinear theory at the instant of time $T = 4\sqrt{h/g}$ following the start of the motion for the following frequencies of the external pressure applied to the free surface: $\alpha_0 = 0.2\sqrt{g/h}$, $0.4\sqrt{g/h}$, $0.6\sqrt{g/h}$, and $0.8g/h$. The figure shows that the influence of the variation of the frequency on the velocity of propagation of the surface waves is negligible and that the fluctuations of the free surface are localized in the same area for the different frequencies. It is also noticed that the amplitudes of the generated waves increase with the inrease of the frequency.

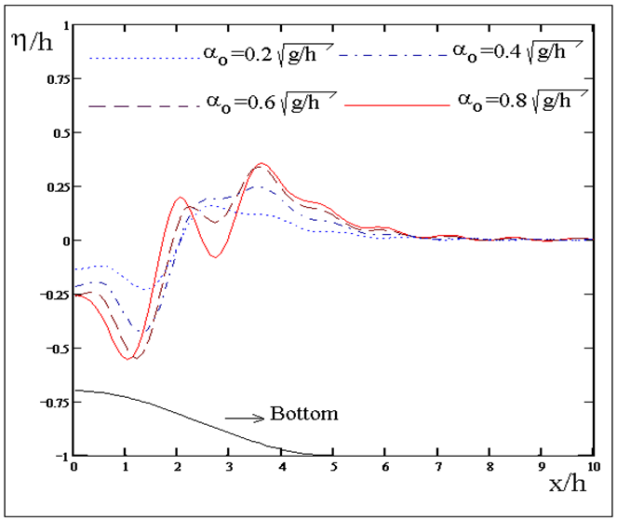

Figure 7. The free surfaces waves over a topography for different values of the frequency according to nonlinear theory. the amplitudes of the generated waves increase with the increase of the frequency.

8.3. Effect of the increase of the area exposed to the external pressure

Figure 8 exhibits the profiles of the free surface calculated according to the nonlinear theory at the instant $T = 4\sqrt{h/g}$ following the start of the motion for the following values of the parameter a, representing half-width of the area on the free surface exposed to the applied external pressure: $a = 2.0h$, $4.0h$, and $6.0h$.

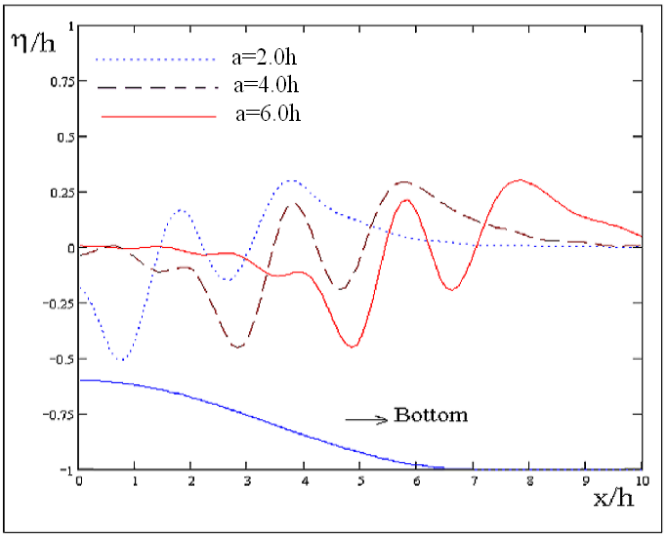

Figure 8. The profiles of the free surface's waves over a topography for different areas exposed to external pressure according to the nonlinear theory. The amplitudes of the generated waves are almost equal, but the larger area exposed to the applied external pressure produces faster waves.

The figure shows that the amplitudes of the generated waves are almost equal, but the larger area exposed to the applied external pressure produces faster waves. We also notice, in all cases, that a part of the free surface lying just above the hump remains at the neighborhood of its position at rest. The width of this part increases with the increase of the width of the area exposed to the external pressure.

9. Concluding remarks

The present work deals with the theoretical aspects of the physical oceanographic phenomenon of generation and propagation of waves in vast oceans with arbitrary topography, due to varying winds blowing on the free surface of the ocean. These winds, interacting with the ocean's free surface, instigate the formation of waves that traverse through waters of varying depths and contours. The study aims to understand the effect of nonlinear theory for the physical mechanisms behind these phenomena, considering the ocean's complex topography which includes underwater features that can alter the course and characteristics of the waves. The following concluding some mathematical results and some physical remarks could be drawn out.

9.1. Some mathematical results

A nonlinear two-dimensional mathematical model is introduced to simulate the intricate process

of wave generation and propagation. Linear and nonlinear theories are formulated, and the corresponding systems of equations and conditions are solved and analyzed. Hince there are several mathematical results of this study that can be formulated as theories to compare the linear theory and the non-linear (quadratic) theory as the following:

Theorem 1. The linear theory may be adequate for describing the phenomenon in a narrow interval of time following the start of the motion, the quadratic theory is necessary for predicting the phenomenon as time elapses.

Theorem 2. The waves calculated following the nonlinear theory are shown to be faster than those calculated according to the linear theory. The above Theorem 2 highlights the critical importance of nonlinear theory for more realistic representation of wave dynamics.

Theorem 3. Linear theory is sufficient to describe the phenomenon only in the cases of low frequencies, however, as frequency increases, the quadratic theory plays vital role for accurate depiction.

Theorem 4. For wide regions, exposed to the external pressure, the free surface in the area just above the corrugated part of the bottom lies in the neighborhood of its position at rest and the outputs of both linear and nonlinear theories converge while as one moves away from this area, a significant difference between the outputs of the two theories appears and the non-linear theory cannot be neglected in this scenario.

Theorem 5. Important fluctuations, of the free surface, characterizing the nonlinear theory features of the flow are screened by the linear theory.

9.2. Some physical remarks according to the nonlinear theory technique

Remark 1. In the course of time, the waves generated inside oceans with irregular topographies, by the effect of oscillating winds blowing on the free surface, increase notably in amplitude and slightly in wavelength. The waves generated on each side of the bottom corrugation, advance slowly towards the corresponding extremity of the channel.

Remark 2. The frequency variations of the winds have a minimal impact on the waves' propagation speed and the fluctuations of the free surface are localized in the same area for different frequencies.

Remark 3. The amplitudes of the generated waves increase slightly by increasing the frequency of the blowing winds. This correlation suggests that the energy imparted by faster wind cycles marginally amplifies the waves' height providing the balance between atmospheric forces and oceanic responses.

Remark 4. For areas of the free surface with different widths, exposed to the blowing winds, the amplitudes of the generated waves are almost equal, but the larger area exposed to these winds give rise to swifter wave velocities. Also, in all cases, a part of the free surface lying just above the corrugated bottom remains at the neighborhood of its position at rest. The width of this part increases with the increase of the width of the area exposed to the winds.

Remark 5. The free surface profiles, corresponding to different bottom topographies, are very near to each other for instants of time following the start of the climate variation, and the effect of the topography on these profiles increases in the course of time. The waves on horizontal bottoms are smaller in amplitude and faster in velocity than those on corrugated bottoms.

Author contributions

Mustafah Abou-Dina: investigation (equal), methodology (equal), resources (equal), software (equal); Amel Alaidrous: conceptualization (equal), data curation (equal), formal analysis (equal), writing-original draft (equal). All authors of this article have been contributed equally. All authors have read and approved the final version of the manuscript for publication.

Use of AI tools declaration

The authors declare they have not used Artificial Intelligence (AI) tools in the creation of this article.

Conflict of interest

The authors declare that they have no conflict of interest.

References

1. B. Le Méhauté, S. Wang, *Water waves generated by underwater explosion*, Singapore: World Scientific, 1996. https://doi.org/10.1142/2587
2. M. S. Abou-Dina, F. M. Hassan, Generation and propagation of nonlinear tsunamis in shallow water by a moving topography, *J. Appl. Math. Comput.*, **177** (2006), 785–806. https://doi.org/10.1016/j.amc.2005.11.033
3. I. R. Young, *Wind generated ocean waves*, Amsterdam: Elsevier, 1999.
4. L. H. Holthuijsen, *Waves in oceanic and coastal waters*, Cambridge: Cambridge University Press, 2007. https://doi.org/10.1017/CBO9780511618536
5. S. R. Jayne, L. C. S. Laurent, S. T. Gille, Connections between ocean bottom topography and Earth's climate, *Oceanography*, **17** (2004), 65–74. https://doi.org/10.5670/oceanog.2004.68
6. L. Chen., J. Y. Yang, L. X. Wu, Topography effects on the seasonal variability of ocean bottom pressure in the North Pacific Ocean, *J. Phys. Oceanogr.*, **53** (2023), 929–94. https://doi.org/10.1175/jpo-d-22-0140.1
7. J. H. Qin, X. H. Cheng, C. C. Yang, N. S. Ou, X. Q. Xiong, Mechanism of interannual variability of ocean bottom pressure in the South Pacific, *Clim. Dyn.*, **59** (2022), 2103–2116. https://doi.org/10.1007/s00382-022-06198-0
8. J. Y. Yang, K. Chen, The role of wind stress in driving the along-shelf flow in the northwest Atlantic Ocean, *J. Geophys. Res. Oceans*, **126** (2021), e2020JC016757. https://doi.org/10.1029/2020JC016757
9. Y. Du, X. L. Dong, X. W. Jiang, Y. H. Zhang, D. Zhu, Q. W. Sun, et al., Ocean surface current multiscale observation mission (OSCOM): Simultaneous measurement of ocean surface current, vector wind, and temperature, *Prog. Oceanogr.*, **193** (2021), 102531. https://doi.org/10.1016/j.pocean.2021.102531
10. A. A. Alaidrous, Transmission and reflection of water-wave on a floating ship in vast oceans, *Comput. Mater. Con.*, **67** (2021), 2071–2988. https://doi.org/10.32604/cmc.2021.015159

11. W. Shi, S. H. Zhang, C. Michailides, L. X. Zhang, P. Y. Zhang, X. Li, Experimental investigation of the hydrodynamic effects of breaking waves on monopiles in model scale, *J. Mar. Sci. Technol.*, **28** (2023), 314–325. https://doi.org/10.1007/s00773-023-00926-9
12. P. Wang, K. Z. Fang, G. Wang, Z. B. Liu, J. W. Sun, Experimental and numerical study of the nonlinear evolution of regular waves over a permeable submerged breakwater, *J. Mar. Sci. Eng.*, **11** (2023), 1610. https://doi.org/10.3390/jmse11081610
13. A. V. Bazilevskii, S. Wongwises, V. A. Kalinichenko, S. Y. Sekerzh-Zen'kovich, Experimental investigation of influence of bottom structure effect on the damping of standing surface waves in a rectangular vessel, *Fluid Dynam.*, **36** (2001), 652–657.
14. F. De Serioa, M. Mossa, Experimental study on the hydrodynamics of regular breaking waves, *Coast. Eng.*, **53** (2006), 99–113. https://doi.org/10.1016/j.coastaleng.2005.09.021
15. M. S. Abou-Dina, Contribution à l'étude de regime transitoire dans les canaux à houles, PhD Thesis, Université de Grenoble, 1983.
16. M. S. Abou-Dina, M. A. Helal, Reduction for the non-linear problem of fluid waves to a system of integro-differential equations with an oceanographic application, J. *Comput. Appl. Math.*, **95** (1998), 65–81. https://core.ac.uk/download/pdf/82146506.pdf
17. M. S. Abou-Dina, M. A. Helal, Boundary integral method applied to the transient, nonlinear wave propagation in a fluid with initial free surface elevation, *Appl. Math. Model.*, **24** (2000), 535–549. https://doi.org/10.1016/S0307-904X(99)00054-2
18. F. M. Hassan, Boundary integral method applied to the propagation of nonlinear gravity waves generated by a moving bottom, *Appl. Math. Model.*, **33** (2009), 451–466. https://doi.org/10.1016/j.apm.2007.11.034
19. H. Lamb, *Hydrodynamics*, 6 Eds., Cambridge: Cambridge University Press, 1932.
20. M. S. Abou-Dina, F. M. Hassan, Approximate determination of the transmission and reflection coefficients for water-wave flow over a topography, *Appl. Math. Comput.*, **168** (2005), 283–304. https://doi.org/10.1016/j.amc.2004.08.019
21. M. S. Abou-Dina, A. F. Ghaleb, Multiple waves scattering by submerged obstacles in an infinite channel of finite depth. I. streamlines, *Eur. J. Mech. B/Fluids*, **59** (2016), 37–51. https://doi.org/10.1016/j.euromechflu.2016.04.005
22. S. L. Cole, Transient wave produced by flow past a bump, *Wave Motion*, **7** (1985), 579–587. https://doi.org/10.1016/0165-2125(85)90035-6
23. A. F. Ghaleb, I. A. Z. Hefni, Wave free, two-dimensional, gravity flow of an inviscid fluid over a bump, *J. Mech. Theor. Appl.*, **6** (1987), 463–488.
24. S. N. Hanna, M. N. Abdel-Malek, M. B. Abd-el-Malek, Super-critical free surface flow over a trapezoidal obstacle, *J. Comput. Appl. Math.*, **66** (1996), 279–291. https://doi.org/10.1016/0377-0427(95)00160-3
25. T. Nakayama, M. Ikegawa, Finite element analysis of flow over a weir, *Comput. Struct.*, **19** (1984), 129–135. https://doi.org/10.1016/0045-7949(84)90211-6
26. R. W. Yeung, Numerical methods in free-surface flows, *Ann. Rev. Fluid Mech.*, **14** (1982), 395–442. https://doi.org/10.1146/annurev.fl.14.010182.002143
27. J. J. Stoker, On radiation conditions, *Commun. Pur. Appl. Math.*, **9** (1956), 577–595. https://doi.org/10.1002/cpa.3160090327
28. J. J. Stoker, *Water waves: The mathematical theory with application*, New York: John Wiley & Sons, Inc., 1957. https://doi.org/10.1002/9781118033159.ch11

29. M. S. Abou-Dina, Nonlinear transient gravity waves due to an initial free surface elevation over a topography, *J. Comput. Appl. Math.*, **130** (2001), 173–195. https://doi.org/10.1016/S0377-0427(99)00384-2
30. M. S. Abou-Dina, M. A. Helal, The influence of a submerged obstacle on an incident wave in stratified shallow water, *Eur. J. Mech. B/Fluids*, **9** (1990), 545–564.
31. M. S. Abou-Dina, M. A. Helal, The effect of a fixed barrier on an incident progressive wave in shallow water, *Nuov. Cim. B*, **107** (1992), 331–344. https://doi.org/10.1007/BF02728494
32. M. S. Abou-Dina, M. A. Helal, The effect of a fixed submerged obstacle on an incident wave in stratified shallow water (mathematical aspects), *Nuov. Cim. B*, **110** (1995), 927–942. https://doi.org/10.1007/BF02722861
33. E. L. Shroye, J. N. Moum, J. D. Nash, Nonlinear internal waves over New Jersey's continental shelf, *J. Geophys. Res. Oceans*, **116** (2011), e2010JC006332. https://doi.org/10.1029/2010JC006332
34. C. A. Whitwell, N. L. Jones, G. N. Ivey, M. G. Rosevear, M. D. Rayson, Ocean mixing in a shelf sea driven by energetic internal waves, *J. Geophys. Res. Oceans*, **129** (2024), e2023JC019704. https://doi.org/10.1029/2023JC019704
35. D. P. Marshall, A theoretical model of long Rossby waves in the southern ocean and their interaction with bottom topography, *Fluids*, **1** (2016), 17. https://doi.org/10.3390/fluids1020017
36. K. Q. Zhang, Analysis of non-linear inundation from sea-level rise using LIDAR data: a case study for south Florida, *Climatic Change*, **106** (2011), 537–565. https://doi.org/10.1007/s10584-010-9987-2
37. J. P. Germain, Théorie générale des mouvements d'un fluide parfait pesant en eau peu profonde de profondeur constante, *C. R. Acad. Sci. Paris Sér. A-B*, **274** (1972), 997–1000.
38. Y. L. Chen, J. B. Hung, S. L. Hus, S. C. Hsiao, Y. C.Wu, Interaction of water waves and a submerged parabolic uniform/shear current using RANS model, *Math. Probl. Eng.*, **2014** (2014), 896723. https://doi.org/10.1155/2014/896723
39. M. A. Spall, Wind-forced seasonal exchange between marginal seas and the open ocean, *J. Phys. Oceanogr.*, **53** (2023), 763–777. https://doi.org/10.1175/JPO-D-22-0151.1
40. N. Soontiens, C. Subich, M. Stastna, Numerical simulation of super critical trapped internal waves over topography, *Phys. Fluids*, **22** (2010), 116605. https://doi.org/10.1063/1.3521532
41. S. Ahmad, S. F. Aldosary, M. A. Khan, Stochastic solitons of a short-wave intermediate dispersive variable (SIdV) equation, *AIMS Mathematics*, **9** (2024), 10717–10733. https://doi.org/10.3934/math.2024523
42. X. Y. Gao, Two-layer-liquid and lattice considerations through a (3+1)-dimensional generalized Yu-Toda-Sasa-Fukuyama system, *Appl. Math. Lett.*, **152** (2024), 109018. https://doi.org/10.1016/j.aml.2024.109018
43. X. Y. Gao, Oceanic shallow-water investigations on a generalized Whitham-Broer-Kaup-Boussinesq-Kupershmidt system, *Phys. Fluids*, **35** (2023), 127106. https://doi.org/10.1063/5.0170506
44. X. Y. Gao, Considering the wave processes in oceanography, acoustics and hydrodynamics by means of an extended coupled (2+1)-dimensional Burgers system, *Chinese J. Phys.*, **86** (2023), 572–577. https://doi.org/10.1016/j.cjph.2023.10.051

45. X. Y. Gao, Y. J. Guo, W. R. Shan, Theoretical investigations on a variable-coefficient generalized forced-perturbed Korteweg-de Vries-Burgers model for a dilated artery, blood vessel or circulatory system with experimental support, *Commun. Theor. Phys.*, **75** (2023), 115006. https://doi.org/10.1088/1572-9494%2Facbf24
46. X. H. Wu, Y. T. Gao, Generalized Darboux transformation and solitons for the Ablowitz-Ladik equation in an electrical lattice, *Appl. Math. Lett.*, **137** (2023), 108476. https://doi.org/10.1016/j.aml.2022.108476
47. Y. Shen, B. Tian, T. Y. Zhou, C. D. Cheng, Multi-pole solitons in an inhomogeneous multi-component nonlinear optical medium, *Chaos Soliton. Fract.*, **171** (2023), 113497. https://doi.org/10.1016/j.chaos.2023.113497
48. T. Y. Zhou, B. Tian, Y. Shen, X. T. Gao, Auto-Bäcklund transformations and soliton solutions on the nonzero background for a (3+1)-dimensional Korteweg-de Vries-Calogero-Bogoyavlenskii-Schif equation in a fluid, *Nonlinear Dyn.*, **111** (2023), 8647–8658. http://dx.doi.org/10.1007/s11071-023-08260-w
49. X. T. Gao, B. Tian, Water-wave studies on a (2+1)-dimensional generalized variable-coefficient Boiti-Leon-Pempinelli system, *Appl. Math. Lett.*, **128** (2022), 107858.
50. X. Bertin, A. de Bakker, A. van Dongeren, G. Coco, G. Andre, F. Ardhuin, et al., Infragravity waves: from diving mechanisms to impacts, *Earth-Sci. Rev.*, **177** (2018), 774–799. https://doi.org/10.1016/j.earscirev.2018.01.002
51. M. Y. Markina, J. H. P. Studholme. S. K. Gulev, Ocean wind waves climate responses to wintertime north Atlantic atmospheric transient eddies and low-frequency flow, *Amer. Meteorolog. Soc.*, **32** (2019), 5619–5638. https://doi.org/10.1175/JCLI-D-18-0595.1
52. C. J. Tranter, *Integral transforms in mathematical physics*, 3 Eds., London: Methuen Co. Ltd., 1966. https://search.worldcat.org/en/title/10766030
53. A. H. Nayfeh, *Introduction to perturbation techniques*, New York: Wiley-Interscience Pub., 1981.
54. M. J. Lighthill, *An introduction to Fourier analysis and generalized functions*, Cambridge: Cambridge University Press, 1958. https://doi.org/10.1017/CBO9781139171427